Electron scattering in Pt(PF$_3$)$_4$: Elastic scattering, vibrational, and electronic excitation

M. Allan

Department of Chemistry, University of Fribourg, chemin du Musée 9, CH-1700 Fribourg, Switzerland

Experimental absolute differential cross sections for elastic scattering, and for vibrational and electronic excitation of Pt(PF$_3$)$_4$ by low-energy electrons are presented. The elastic cross sections have a deep angle-dependent Ramsauer-Townsend minimum ($E_{min} = 0.26$ eV at $\theta = 135°$). The angular distributions of the elastic cross section at and above 6.5 eV show an unusually narrow peak at an angle which decreases with increasing energy (it is at 40° at 20 eV). Wavy structure is observed at higher angles at 15 and 20 eV. Vibrational excitation cross sections reveal five shape resonances, at 0.84, 1.75, 3.3, 6.6, and 8.5 eV. The angular distributions of the vibrational cross sections have a strong forward peak and are nearly isotropic above about 60°. Electronically excited states are characterized by electron energy-loss spectra. They show a number of unstructured bands, the lowest at 5.8 eV. They are assigned to Rydberg states converging to the 1st and 2nd ionization energies. The cross sections for electronic excitation have very high forward peaks, reaching the value of 50 Å^2 at 50 eV and 0° scattering angle. Purity of the sample was monitored by the very low frequency (26 meV) Pt−P stretch vibration in the energy-loss spectra.

I. INTRODUCTION

The interest in electron interactions with Pt(PF$_3$)$_4$ was motivated by its use as a platinum precursor for the deposition of nano-sized wires in the method of focused electron beam induced processing (FEBIP).[1] It has the advantage, over precursors with carbon-containing ligands, of yielding carbon-free deposits.[2] The strive to improve the quality of the FEBIP-generated material, in particular increasing the conductivity of the deposited nanowires and improving the spatial resolution, leads to a desire to understand the mechanism of the deposition process. The pertinent questions are what are the roles of the various decomposition processes—dissociative ionization, neutral dissociation, dissociative electron attachment, bipolar dissociation and possibly local thermal decomposition. Another important question is whether the majority of the deposition is performed by the very fast primary electrons, or by the "early," still very fast secondary electrons, or by the many slow secondary electrons which form the end of the "shower" resulting from an impact of a fast primary electron.

This work is concerned with the study of elastic scattering and of vibrational and electronic excitation by electron impact. Electronic excitation is likely to lead to dissociation of the target molecule. But even electron collision processes not leading to dissociation are relevant for FEBIP—elastic scattering changes the directions of the incoming electrons and thus broadens the electron beam, and vibrational excitation cools the electrons and heats the sample.

Although this work was originally motivated by the desire to contribute to the understanding of the FEBIP application, the study is interesting also from a purely scientific point of view, Pt(PF$_3$)$_4$ being a very unusual molecule. It is a tetrahedral d^{10} complex.[3] It is very unusual that a molecule with such a high mass (547 amu) is volatile enough to be measured in the present instrument, limited to room temperature—in fact keeping the sample at 0 °C was enough to generate sufficient vapor pressure. The unusual bonding in Pt(PF$_3$)$_4$ is reflected in the vibrational frequencies. The lowest vibrations, P−Pt−P deformations have frequencies of only 6 meV and can not be resolved in the present experiment. This low frequency shows that the PF$_3$ ligands move nearly freely laterally on the surface of the Pt atom. The Pt−P stretch vibrations have frequencies of only 26 meV, reflecting a very weak Pt−P bond.

II. EXPERIMENT

The measurements were performed with a spectrometer using hemispherical analyzers.[4–7] The energy resolution was about 14 meV in the energy-loss mode, at a beam current of around 200 pA. The energy of the incident beam was calibrated on the 19.365 eV (Ref. 8) ^{2}S resonance in helium and is accurate to within ±10 meV. The instrumental response function was determined on elastic scattering in helium and all spectra were corrected as described earlier.[5,7] Absolute values of the cross sections were determined by the relative flow technique as described by Nickel *et al.*[9] using the theoretical helium elastic cross sections of Nesbet[10] as a reference. The confidence limit is about ±20% for the elastic cross sections and ±25% for the inelastic cross sections (two standard deviations). During the absolute measurements background was determined by recording signal with gas flowing into the main chamber *via* a by-pass line instead by the nozzle. This background was generally negligible except in the more forward scattering and at low energies—but for consistency the "by-pass signal" was subtracted even when it was very low.

The angular distributions were measured using combined mechanical setting of the analyzer and magnetic deflection using the magnetic angle changer,[11, 12] correcting the curves for the instrumental response function, and fitting them to the discrete absolute values measured at $45°$, $90°$, $135°$, and $180°$, as described in references.[5, 7] The angle of the magnetic scan was incremented in steps of $2.5°$.

The sample was purchased from STREM Chemicals in a sealed ampule under PF_3 gas. The excess PF_3 was removed by pumping while keeping the test tube at $-20\,°C$. The sample purity during this process was monitored by electron energy loss spectra as described in the Appendix. $Pt(PF_3)_4$ initially caused the potentials within the instrument to drift dramatically, after 1-2 weeks they stabilized sufficiently to allow the measurements, but with frequent recalibration of the energy scales. $Pt(PF_3)_4$ decomposed on even moderately hot surfaces in the instrument, primarily around the filament, and covered them by a silvery layer, presumably metallic platinum. This layer deposited also on the ruby balls used as insulating spacers between the electron-optics elements, short circuiting them. This process was slow enough, however, to permit measurements for several weeks. Partial short circuit does not affect the operation of the instrument because all voltages are supplied by operational amplifiers with low output impedance, so that the voltage does not drift even when current is drawn by a partial short circuit.

III. ELASTIC SCATTERING

The elastic cross sections are shown, as a function of energy, for several representative angles, in Fig. 1. Striking is a deep Ramsauer-Townsend minimum. It is observed at 0.75 eV at $45°$, 0.36 eV at $90°$, 0.26 eV at $135°$, and 0.24 eV at $180°$. A number of further minima appear at higher energies, similarly to, for example, Kr.[13] The three relatively narrow peaks which appear at 0.8, 1.5, and 3.3 eV in the $135°$ spectrum can be assigned to resonances, which will be discussed in more detail below in connection with vibrational excitation. Most of the structure in the elastic cross sections
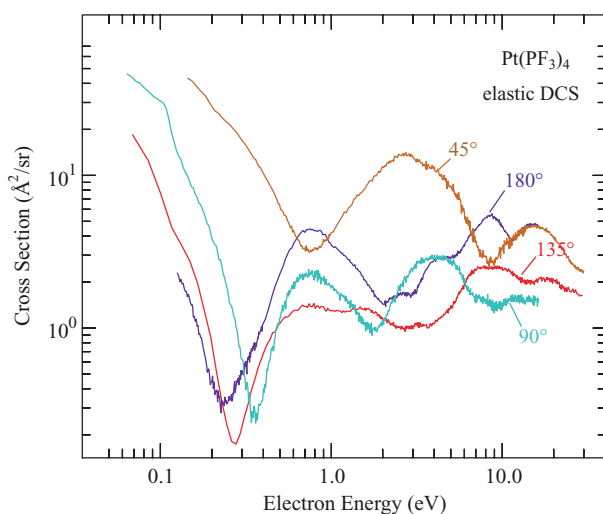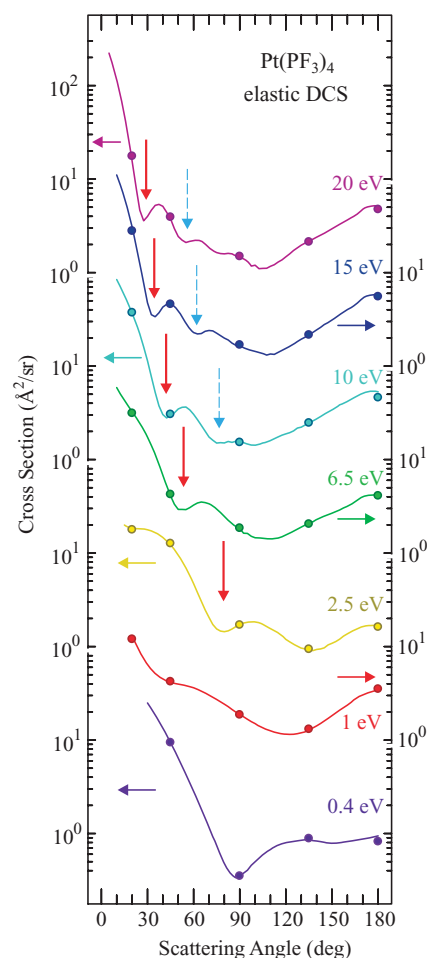

FIG. 2. Angular scans of the elastic cross sections. Horizontal arrows relate the curves with the appropriate vertical scale. Vertical arrows point to narrow dips in the cross section.

is a result of interferences of various partial waves, however, and cannot be associated with resonances. A downward step can be discerned at 0.112 eV in the $135°$ cross section which could be a cusp or a vibrational Feshbach resonance.

Figure 2 shows an overview of the angular distributions of the elastic cross sections. The circles show the results of individual absolute measurements, obtained by normalization to the helium cross sections. The continuous lines show the results of magnetic angular scans (in steps of $2.5°$), corrected by the instrumental response function and normalized to the absolute measurements. In principle, only one absolute measurement would be required to normalize each angular scan, but the agreement of the angular scan with several (4 or 5) absolute points represents a useful test of the correctness of the angular response correction.

The cross sections exhibit a number of minima with interesting trends. Only one minimum appears at 0.4 eV, two minima appear at and above 2.5 eV. They are marked by vertical arrows in Fig. 2 and shift to lower angles with increasing energy. A third minimum appears weakly at 20 eV, giving the angular distribution a wavy aspect. The cross sections have a strong forward peak at higher energies.

The angular structures are surprisingly narrow for angular distributions from molecules. This is visible very clearly

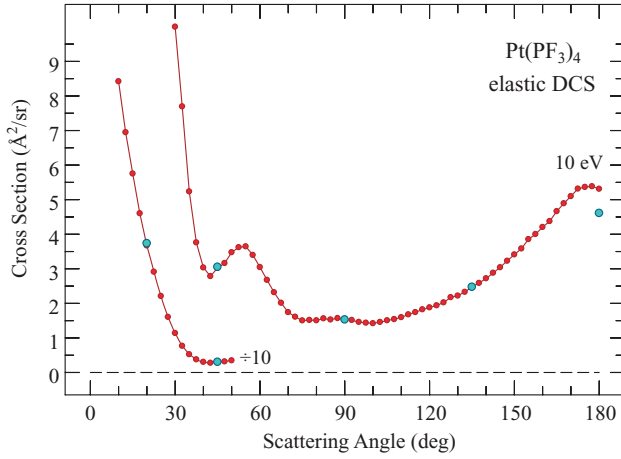FIG. 1. Energy scans of the elastic cross sections.

2

FIG. 3. Elastic cross section at 10 eV.

in Figs. 3 and 4, which show two cross sections on a linear scale. The narrowest structures are only about 15° wide. Part of the explanation is presumably that $Pt(PF_3)_4$ is a "quasi-spherical" molecule, both because most of the electrons are in the spherical Pt atom, and because the PF_3 ligands are arranged in a highly symmetrical tetrahedral manner. The cross sections are thus likely to depend only weakly on the orientation of the target and are not smeared out by the random target orientations. Integral cross sections derived from the angular distributions (with visual extrapolation to $0°$) are given in Table I.

IV. VIBRATIONAL EXCITATION

A. Energy-loss spectra

One important outcome from studying vibrational excitation is the characterization of resonances[14] and the first step consists of determining which vibrational modes play a key role. This can be seen in the representative vibrational energy-loss spectrum shown in Fig. 5. It was recorded with a slightly higher resolution of 10 meV. The incident energy of 0.7 eV was chosen to correspond to a shape resonance, which will be
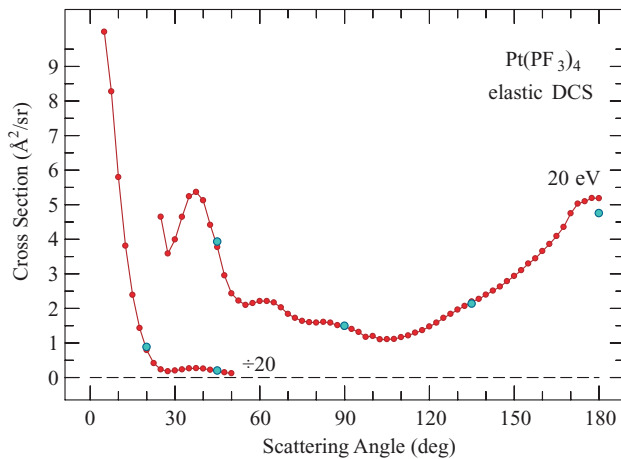

FIG. 4. Elastic cross section at 20 eV.

TABLE I. Integral elastic cross sections, ±20%.

Energy	0.4 eV	1.0 eV	2.5 eV	6.5 eV	10 eV	15 eV	20 eV
ICS ($Å^2$)	70.7	39.5	57.1	64.3	64.7	66.8	59.8

discussed in more detail in Sec. IV B. Four vibrational losses, together with their overtones and combinations, can be discerned and compared to the known vibrational frequencies from Ref. 3, reproduced in Table II. Although the observed energy-losses can generally not be uniquely assigned to individual vibrations, they can be assigned to a given type. The 26 meV energy-loss is due to the Pt−P stretch vibration, either ν_3 or ν_{18}. The 48 meV energy-loss is due to the PF_3 deformation vibration, primarily to ν_{16}. The 65 meV energy-loss is due to another type of PF_3 deformation vibration, ν_2 and/or ν_{15}. The 113 meV energy-loss is due to the P−F stretch vibration, ν_1 and/or ν_{13}. The 6 meV PtP_4 deformation vibrations ν_8 and ν_{19}, both degenerate, are not resolved and only broaden the elastic peak. These two and the other low-frequency vibrations are strongly excited thermally, as manifested also by the intense superelastic peaks. This paper adopts the pragmatic approach of not attempting to unravel the individual contributions of the vibrationally excited target.

The weakness of the Pt−P bond has the consequence that those $Pt(PF_3)_4$ vibrations which are largely localized on the PF_3 ligand have similar frequencies as free PF_3 so that free PF_3 and the Pt complex can not be distinguished with the present resolution. In fact, only the 26 meV energy-loss is a unique evidence of the presence of $Pt(PF_3)_4$. (The absence of free PF_3 can be concluded from a near-disappearance of the elastic signal at the Ramsauer-Townsend minimum—see the Appendix).

TABLE II. Vibrational frequencies of $Pt(PF_3)_4$ from Ref. 3.

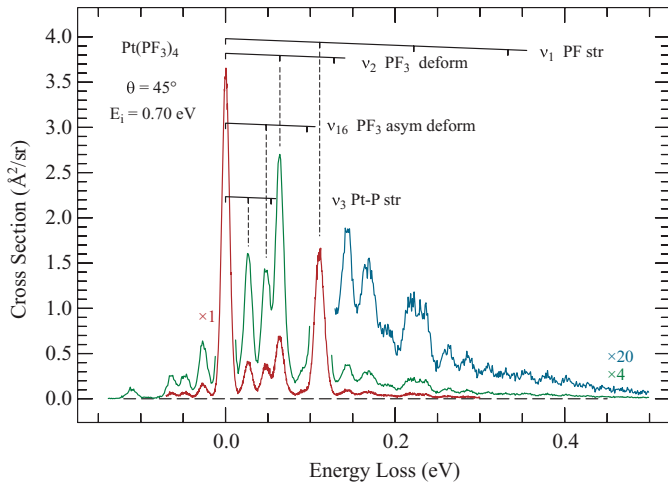| Symm	No.	Description	Energy (meV)
A_1	ν_1	PF symm str	119
	ν_2	PF_3 symm def	68
	ν_3	Pt-P symm str	26
E	ν_4	PF_3 torsion	18
	ν_5	PF asymm str	106
	ν_6	PF_3 asymm def	41
	ν_7	PF_3 rock	35
	ν_8	PtP_4 deform	6
F_1	ν_9	PF asymm str	106
	ν_{10}	PF_3 asymm def	43
	ν_{11}	PF_3 rock	34
	ν_{12}	PF_3 torsion	18
F_2	ν_{13}	PF symm str	112
	ν_{14}	PF asymm str	107
	ν_{15}	PF_3 symm def	64
	ν_{16}	PF_3 asymm def	48
	ν_{17}	PF_3 rock	35
	ν_{18}	Pt-P asymm str	27
	ν_{19}	PtP_4 def	6

3

FIG. 5. Electron energy-loss spectrum.

B. Vibrational excitation—energy scans

The cross sections for the four energy-losses identified in Sec. IV A were measured as a function of energy at representative angles and are shown in Figs. 6–9. It is well known[14] that vibrational excitation cross sections by electron impact are generally very small (as a consequence of the very small mass of the electron as compared to that of the nuclei), except for direct dipole excitation of IR vibrations at low energies and forward scattering angles, and for resonant excitation, which occurs at the energy of the resonance and is generally pronounced also at large angles. To study resonances, it is therefore advantageous to regard the cross sections at large

FIG. 7. Energy scans of the vibrational excitation cross sections recorded at $\theta = 135°$.

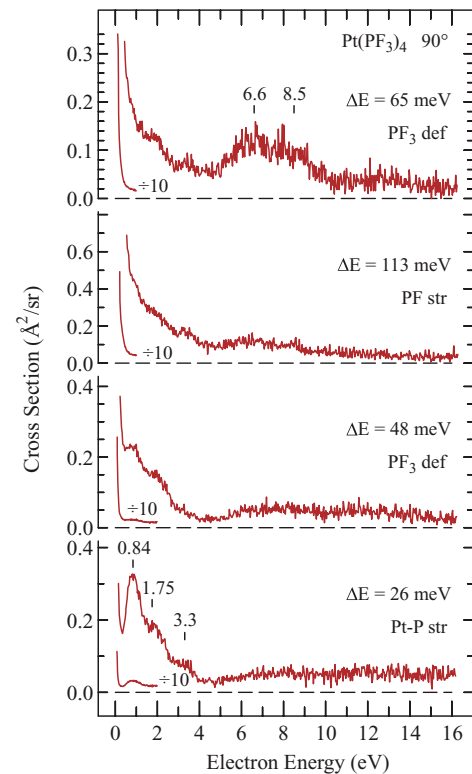FIG. 6. Energy scans of the vibrational excitation cross sections recorded at $\theta = 180°$.

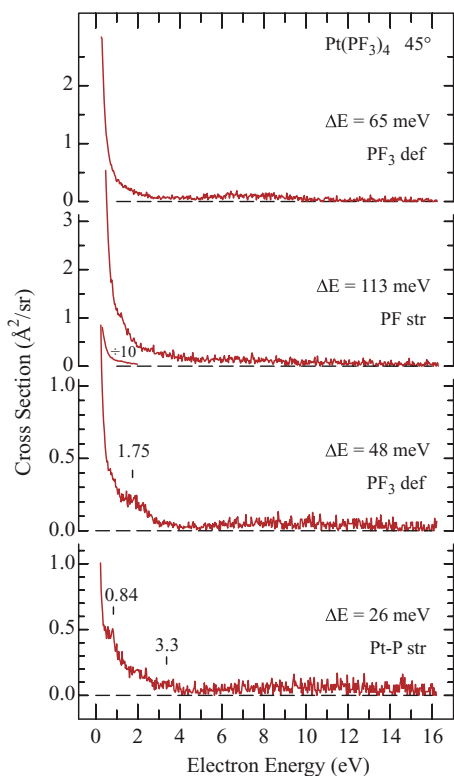FIG. 8. Energy scans of the vibrational excitation cross sections recorded at $\theta = 90°$.

FIG. 9. Energy scans of the vibrational excitation cross sections recorded at $\theta = 45°$.

angles, where the direct mechanism does not interfere, and the 180° cross sections are therefore presented first, in Fig. 6. The other useful concept is that of characterizing resonances based on the selectivity of exciting the various vibrational modes—the antibonding properties of the orbital temporarily occupied in the (shape) resonance lead to relaxation of the positions of the nuclei and excitation of the modes which correspond to this relaxation (See Ref. 15 for a pioneering study). Finally, vibrational excitation is sensitive primarily to shape resonances (as opposed to core excited resonances).

With these points in mind, five resonances can be identified, marked by vertical bars in Fig. 6. The lower three resonances appear in all three cross sections, in particular also in the Pt−P stretch excitation, indicating that the temporarily captured electron is distributed over the whole molecule, in-
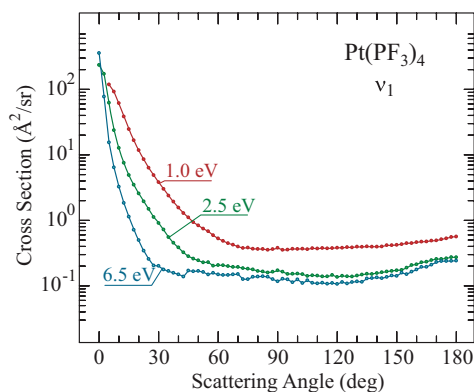
cluding the Pt atom. The observation that the lowest of the three, at 0.84 eV, is most intense is quite common and is generally a consequence of a shorter lifetime (due to faster autodetachment) of the higher-lying resonances, permitting less nuclear relaxation. The two higher-lying resonances, at 6.6 and 8.5 eV, appear with a cross section of about 0.2 Å²/sr in the P−F stretch and the PF$_3$ deformation vibrations, but are missing in the Pt−P stretch vibration, indicating that they are localized on the ligands. The cross sections rise steeply at low energies, near threshold, possibly indicating a virtual state at zero energy (see for example the review in Ref. 16 and references therein for discussion of virtual states and other threshold phenomena).

The cross sections recorded at 135° (Fig. 7) are very similar in shape, and only slightly smaller than those at 180°. This decrease will be clearly visible in the angular scans presented in Sec. IV C. The cross sections recorded at 90° (Fig. 8) start to be different—the lower three resonances are clearly visible only in the Pt−P stretch excitation, and the 6.6 and 8.5 eV resonances only in the topmost trace, the 65 meV PF$_3$ deformation excitation. In the other instances, the resonant structure starts to be hidden under a gradual increase of the cross section with decreasing energy, due doubtlessly to direct dipole excitation. The large cross sections at low energies completely dominate the spectra at 45° in Fig. 9.
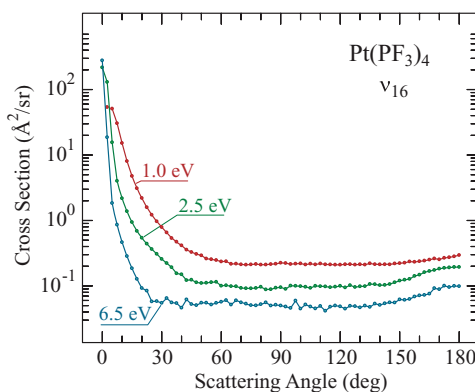

FIG. 11. Angular distribution of the excitation of the ν_2 vibration.

FIG. 10. Angular distribution of the excitation of the ν_1 vibration.

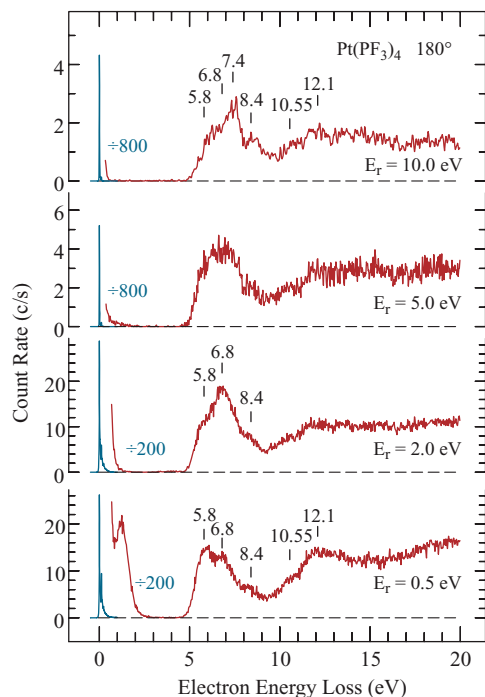FIG. 12. Angular distribution of the excitation of the ν_{16} vibration.

5

FIG. 13. Electron energy loss spectra recorded at 180° with the constant residual energies indicated.

C. Vibrational excitation—angular scans

The cross sections for three energy-losses were measured as a function of scattering angle at representative energies and are shown in Figs. 10–12. The same general pattern is found for all—the cross sections are nearly flat in the intermediate angular range, rise slightly in the backward direction, and rise dramatically in the forward direction. This rise in the forward direction spans around three orders of magnitude and extends over a larger angular range at low energies. These observations are compatible with a nearly isotropic resonant excitation.
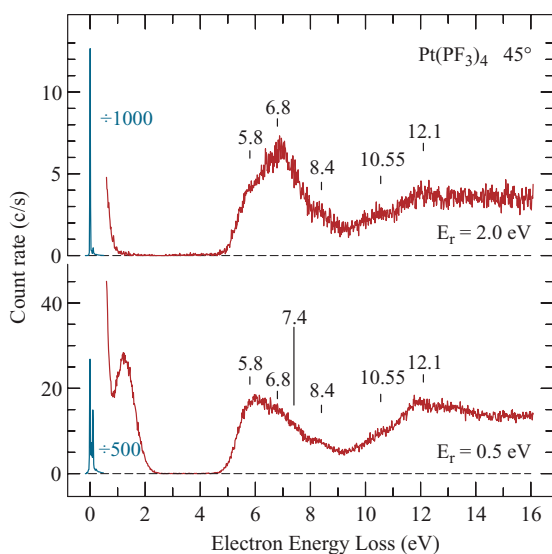

FIG. 14. Electron energy loss spectra recorded at 45° with the constant residual energies indicated.
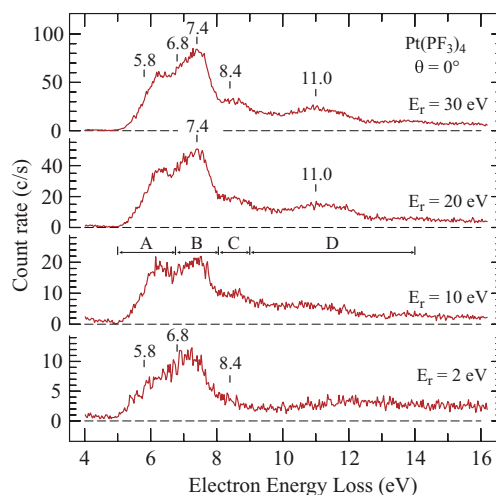

FIG. 15. Electron energy loss spectra recorded at 0° with the constant residual energies indicated. Vertical bars and the letters A-D indicate the energy ranges within which integration was performed to obtain absolute values.

tion, overshadowed by a direct excitation mechanism at forward scattering angles.

V. ELECTRONIC EXCITATION

A. Electronic energy-loss spectra

Similarly to the vibrational excitation, excitation of forbidden electronic transitions is favored at low electron energies and large scattering angles, direct excitation of allowed transitions dominates in the forward direction and at higher
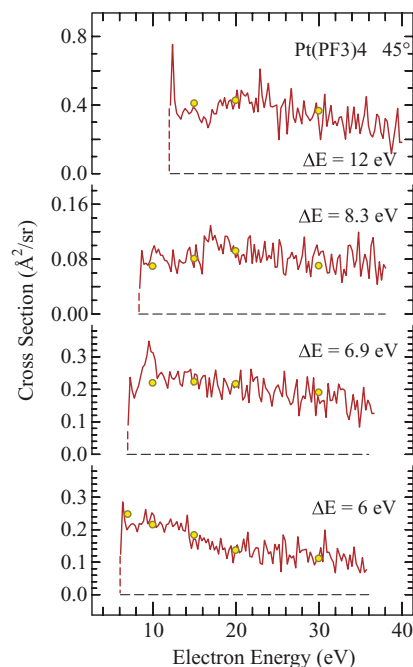

FIG. 16. Energy scans of the cross sections recorded at 45° at the energy losses indicated. The absolute values refer to integrals within the energy-loss ranges A, B, C, and D (bottom to top), indicated in Fig. 15. The (yellow) circles show individual absolute measurements obtained by comparison to the He elastic cross section; the solid (red) lines are the energy scans, normalized to the (yellow) circles.
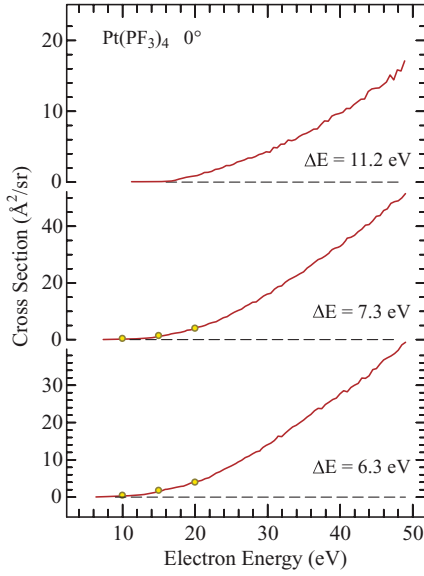
6

FIG. 17. Energy scans of the cross sections recorded at $0°$ at the energy losses indicated. The absolute values refer to integrals within the energy-loss ranges A, B, D, indicated in Fig. 15. The (yellow) circles show individual absolute measurements derived from the angular scans.

FIG. 18. Angular scans of the cross sections recorded at the energies indicated. The absolute values refer to integrals within the first energy-loss range (A) indicated in Fig. 15, i.e., $\Delta E = 5.0 - 6.75$ eV. The (yellow) circles show individual absolute measurements derived from spectra recorded with constant incident energies.

energies. Overview of the transitions is thus provided by a series of energy-loss spectra recorded at various energies and scattering angles. To keep a "unique physical character" across a large energy-loss range, it is more advantageous to record the whole spectrum at a given energy above threshold, that is, at a constant residual energy. Such spectra are presented in Figs. 13–15. All spectra are characterized by broad structureless bands about three orders magnitude weaker than the elastic peak. (The elastic peak cannot be measured at $0°$.) The band at about 1.25 eV in the spectra recorded with $E_r = 0.5$ eV at $45°$ and $180°$ is not due to an electronically excited state but to "unspecific" vibrational excitation (see for example the review[17]) via the 1.75 eV resonance discussed in Sec. IV. (Note that an energy-loss of 1.25 eV and a residual energy of 0.5 eV means that the incident energy is 1.75 eV at the top of the peak—corresponding to the 1.75 eV of the resonance.) The relative intensities of the electronic bands vary with the scattering angle and residual energy, but not to a degree which would permit clear distinction between allowed and forbidden transitions.

The He-I photoelectron spectrum of $Pt(PF_3)_4$ (Ref. 18) consists of broad structureless bands, whose band shapes and widths resemble the present energy-loss bands. The ground state configuration of Pt in $Pt(PF_3)_4$ is $5d^{10}$. The two lowest photoelectron bands are at 9.83 and 12.45 eV and correspond to ionizations from the t_2 and e orbitals, respectively, located predominantly on the Pt atom.[18] Making a reasonable estimate of the term energy to be 4 eV for the lowest Rydberg state leads to an expectation of about 5.8 eV for the lowest energy, in good agreement with the observed 5.8 eV band. The energy-loss bands at 6.8 and 7.4 eV could be higher-lying Rydberg states converging to the same ionization energy (t_2). The energy-loss band at 8.4 eV is likely to be the lowest Rydberg state converging to the 2nd ionization energy, at 12.45 eV (e).
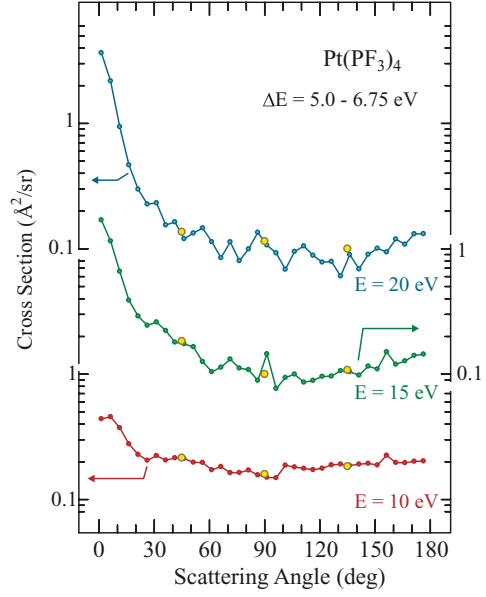
B. Electronic excitation cross sections—energy scans

The cross sections for electronic excitation are shown as a function of electron energy in Figs. 16 and 17. The excitation functions were recorded at the energy-losses indicated in the figures. There is a problem with normalization to absolute values, however, because the individual energy-loss bands are greatly overlapping, and it was not possible to give a cross section for each individual electronically excited state. The pragmatic choice was made to divide the energy-loss range into the sections A, B, C, and D, indicated above the 2nd spectrum from bottom in Fig. 15. The excitation functions in Figs. 16 and 17 were then normalized such as to indicate absolute values for all energy-losses within each of the ranges A-D.

The cross sections recorded at $45°$ (Fig. 16) have a step-wise rise at threshold and then remain nearly constant over a large energy range. At $0°$ the cross sections rise gradually and reach very high values at 50 eV.

C. Electronic excitation cross sections—angular scans

The angular distributions of the cross sections summed within the energy-loss ranges A, B and C defined above, and for three representative incident electron energies, are shown

TABLE III. Integral cross sections for electronic excitations in the energy-loss range $\Delta E = 5 - 9$ eV, $\pm 25\%$.

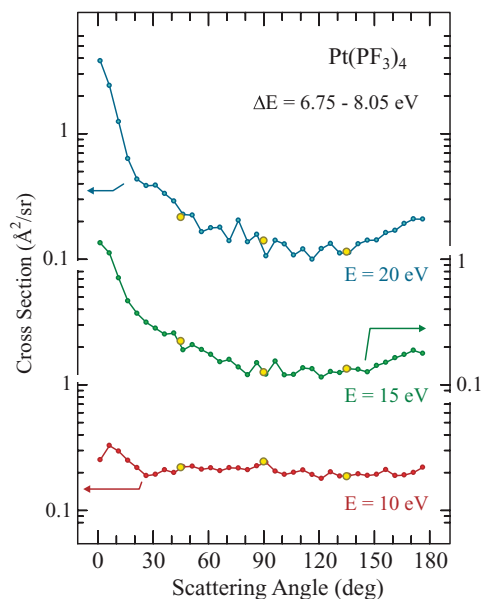| Energy	10 eV	15 eV	20 eV
ICS (Å^2)	5.63	4.71	5.22

FIG. 19. Angular scans of the cross sections recorded at the energies indicated. The absolute values refer to integrals within the second energy-loss range (B) indicated in Fig. 15, i.e., $\Delta E = 6.75 - 8.05$ eV.

FIG. 21. Electron energy-loss spectra which illustrate the decrease of the amount of free PF_3 in the sample during the initial pumping. The upper spectrum was recorded with a partially purified sample, with the sample test tube being kept at $-20\,°$C. The lower spectrum was recorded after additional pumping of 30 min with sample at $-20\,°$C. The sample was warmed to $0\,°$C before recording the lower spectrum.

in Figs. 18–20. They are nearly exactly isotropic near threshold, *i.e.*, at $E = 10$ eV and the energy-loss ranges B and C. (the cross section rises slightly near $0°$ at 10 eV for the energy-loss range A in Fig. 18, but this is presumably because 10 eV is already significantly higher above threshold than for the ranges B and C) At higher incident electron energies the cross sections rise slightly at backward angles and rise dramatically towards $0°$. This is consistent with the very large cross sections observed at $0°$ in Fig. 17. Integration under the angular distributions yields the integral cross sections (ICS) listed in Table III.
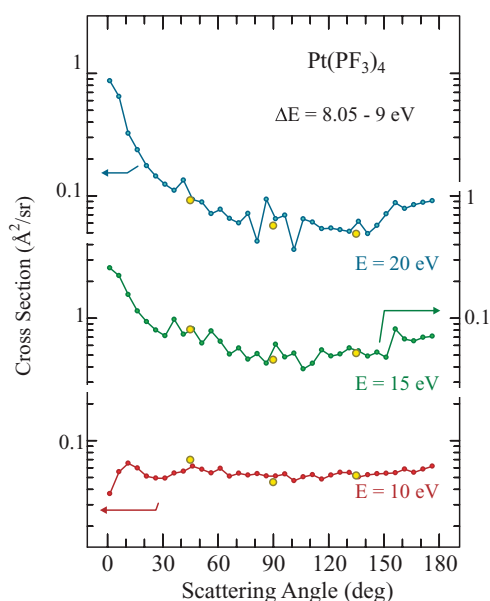

FIG. 20. Angular scans of the cross sections recorded at the energies indicated. The absolute values refer to integrals within the third energy-loss range (C) indicated in Fig. 15, i.e., $\Delta E = 8.05 - 9.0$ eV.
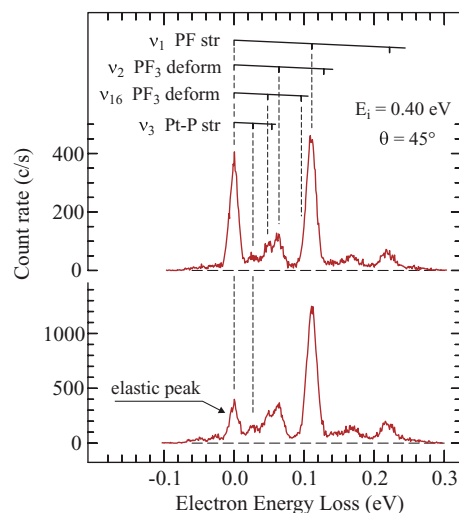
The absolute values of the cross sections are quite large when compared to, for example, those for the excitation of the lowest triplet state of ethene, which is 0.66 $Å^2$ at its peak at 7 eV. [19] Another comparison can be made with the recently measured cross sections for the excitation of the three lowest Rydberg states in tetrahydrofuran (THF) by Do *et al.* [20] Do *et al.* report an ICS of 0.505 $Å^2$ for the excitation of the three lowest Rydberg states at 20 eV. This is about $10\times$ less than the present ICS for the excitation of all electronic states in the energy-loss range 5-9 eV.

It can only be speculated why the present cross sections are that large. One point is that already the elastic ICS of $Pt(PF_3)_4$, 60 $Å^2$, is much larger than that of THF, 30.9 $Å^2$ (both at 20 eV). A second point is that there are certainly many more final states, many of them triply degenerate, in the present energy-loss range (5-9 eV for the data in Table III) than the 3 Rydberg states in THF in the paper of Do *et al.* Finally, the very high forward peak in the present DCSs makes a noticeable contribution to the ICS.

VI. CONCLUSIONS

Despite the many limitations encountered in the effort of using the present data to better understand the decomposition of $Pt(PF_3)_4$ under FEBIP conditions (gas phase vs. condensed phase, the presence of fast primary electrons in FEBIP, presence of partially fragmented molecules in FEBIP, etc.), several useful conclusions can be drawn. A result relevant for FEBIP is that the electronic excitation cross sections reach very large values at higher energies and near-forward scattering. This indicates, under the plausible assumption that the excited states dissociate, an efficient dissociation channel without great broadening of the electron beam. The vibrational excitation cross sections are large at energies below 10 eV,

providing for heating of the sample by slow secondary electrons.

An remarkable observation of purely scientific interest is that the elastic cross sections exhibit surprisingly narrow and repetitive structures in the angular distributions above 10 eV.

APPENDIX: MONITORING SAMPLE PURITY

Monitoring sample purity is important because there is the danger of an admixture of free PF_3. This problem has already been encountered in the past while measuring He-I photoelectron spectra.[18,21] As already mentioned, the majority of the vibrational energy-loss peaks have frequencies which do not distinguish free PF_3 and the $Pt(PF_3)_4$ complex. The only exception is the $Pt-P$ stretch peak at an energy-loss of 26 meV. The energy-loss spectra thus indicate whether $Pt(PF_3)_4$ is present and whether its proportion has stabilized. It does not, however, *a priori* indicate, whether free PF_3 is absent. This can, however to a large degree be deduced from a very low elastic signal at the Ramsauer-Townsend minimum of $Pt(PF_3)_4$ (see Sec. III) as illustrated by the energy-loss spectra in Fig. 21. The sample from a freshly opened ampule was transferred under Ar to a test tube which was then cooled to $-20\,°C$. Gas was admitted to the instrument by a regulating valve and its energy-loss spectra were continuously measured. The initial energy-loss spectra had only a very weak signal at $\Delta E = 26$ meV, but this signal increased with time. At the same time, the total pressure decreased as the PF_3 was removed, and the regulating valve was gradually opened. A spectrum recorded after about one hour is shown at the top of Fig. 21. The disappearance of free PF_3 was then monitored as a decreasing intensity of the elastic peak, which has finally stabilized at a very small value after another half hour of pumping as shown by the lower trace of Fig. 21. The temperature of the sample was increased to 0 °C for the main measurements.

[1]I. Utke, P. Hoffmann, and J. Melngailis, J. Vac. Sci. Technol. B **26**, 1197 (2008).

[2]M. H. Ervin, D. Chang, B. Nichols, A. Wickenden, J. Barry, and J. Melngailis, J. Vac. Sci. Technol. B **25**, 2250 (2007).

[3]R. M. Bligh-Smith, H. G. M. Edwards, and V. Fawcett, Spectrochim. Acta **43A**, 1069 (1987).

[4]M. Allan, J. Phys. B **25**, 1559 (1992).

[5]M. Allan, J. Phys. B **38**, 3655 (2005).

[6]M. Allan, J. Phys. B **40**, 3531 (2007).

[7]M. Allan, Phys. Rev. A **81**, 042706/1 (2010).

[8]A. Gopalan, J. Bömmels, S. Götte, A. Landwehr, K. Franz, M. W. Ruf, H. Hotop, and K. Bartschat, Eur. Phys. J. D **22**, 17 (2003).

[9]J. C. Nickel, P. W. Zetner, G. Shen, and S. Trajmar, J. Phys. E **22**, 730 (1989).

[10]R. K. Nesbet, Phys. Rev. A **20**, 58 (1979).

[11]F. H. Read and J. M. Channing, Rev. Sci. Instrum. **67**, 2373 (1996).

[12]M. Zubek, N. Gulley, G. C. King, and F. H. Read, J. Phys. B **29**, L239 (1996).

[13]O. Zatsarinny, K. Bartschat, and M. Allan, Phys. Rev. A **83**, 032713 (2011).

[14]G. J. Schulz, Rev. Mod. Phys. **45**, 423 (1973).

[15]I. C. Walker, A. Stamatovic, and S. F. Wong, J. Chem. Phys. **69**, 5532 (1978).

[16]H. Hotop, M.-W. Ruf, M. Allan, and I. I. Fabrikant, Adv. At., Mol., Opt. Phys. **49**, 85 (2003).

[17]M. Allan, J. Electron Spectrosc. Relat. Phenom. **48**, 219 (1989).

[18]P. J. Bassett, B. R. Higginson, D. R. Lloyd, N. Lynaugh, and P. J. Roberts, J. Chem. Soc. Dalton Trans. **1974**, 2316 (1974).

[19]M. Allan, C. Winstead, and V. McKoy, Phys. Rev. A **77**, 042715 (2008).

[20]T. P. T. Do, M. Leung, M. Fuss, G. Garcia, F. Blanco, K. Ratnavelu, and M. J. Brunger, J. Chem. Phys. **134**, 144302 (2011).

[21]J. C. Green, D. I. King, and J. H. D. Eland, J. Chem. Soc. D: Chem. Comm. **1970**, 1121 (1970).